Molecular imaging of epidermal growth factor receptor in live cells with refractive index sensitivity using dark-field microspectroscopy and immunotargeted nanoparticles

Adam C. Curry
Matthew Crow
Adam Wax
Duke University
Department of Biomedical Engineering
and Fitzpatrick Institute of Photonics
Durham, North Carolina 27708
E-mail: a.wax@duke.edu

Abstract. We present a study using plasmonic nanoparticles (NPs) to image epidermal growth factor receptor (EGFR) in live cells. Through detailed analysis of the NP scattering spectra, we determine the intracellular refractive index (RI) within attoliter volumes inside of the living cells. Molecular imaging is demonstrated using anti-EGFR labeled gold nanospheres delivered to cancer cells that overexpress EGFR, with targeted binding confirmed by appropriate control experiments. RI determination is achieved by measurement of the bound NPs' scattering spectra, acquired using a precision dark-field microspectroscopy system and through careful characterization of the NP properties throughout the immuno-labeling procedure. To demonstrate the effect of receptor-mediated uptake, the data are compared to similar spectral measurements using antibody-free NPs, taken up by the cells through nonspecific mechanisms. In these experiments, NP aggregation introduces interparticle effects in the scattering spectra, suggesting that EGFR-mediated internalization of NPs may provide an advantage for maintaining NP isolation upon uptake. The results of this study show the potential utility of dark-field microspectroscopy and labeled NPs for live cell imaging. By demonstrating RI sensitivity over nanometer length scales, this study also presents a potential new avenue for assessing the structure and dynamics of live cells. [DOI: 10.1117/1.2837450]

Keywords: molecular imaging; nanoparticles; cell diagnostics; dark-field microscopy.

Paper 07086RR received Mar. 5, 2007; revised manuscript received Aug. 3, 2007; accepted for publication Sep. 4, 2007; published online Feb. 7, 2008.

1 Introduction

Plasmonic nanoparticles (NPs) have been recently discovered as optical contrast agents that offer significant advantages over alternative markers. NPs can be brighter than chemical fluorophores and quantum dots,[1] they are very stable and noncytotoxic,[2–4] and they are not susceptible to photobleaching.[1,5] They also exhibit large scattering cross sections, yielding high contrast and permitting easy localization under dark-field illumination. These properties make NPs ideal for the interrogation of various biological interactions.[6–8] However, the application of NP scattering to molecular imaging has yet to exploit the fact that their scattering and absorption spectra depend strongly on the refractive index of their nanoenvironment,[9] indicating their potential use as intracellular biosensors.

The refractive index (RI) inside a living cell can vary significantly, depending on the composition of the intracellular region. For example, lipid-rich membranes,[10–12] water-rich cytoplasm,[11,13,14] and protein-rich nuclei[13,14] each influence the local RI on nanometer length scales. This dependence suggests that knowledge of the RI may be exploited to indicate intracellular location. In addition, because RI varies with solute concentration,[15,16] it may be exploited as an indicator of biological function. To identify and determine such relationships, an innocuous intracellular RI sensor is needed. Plasmonic NPs, whose resonance spectra depend on the RI of their nanoenvironment, are a promising candidate for such a sensor.

Previous cellular RI measurements have been typically accomplished through spatially averaged measurements, determined by changes in optical path length through live cells.[17,18] However, these methods cannot selectively determine the RI of intracellular regions of interest. As an exception, a recent experiment was able to determine intracellular RI using fluorescence lifetime imaging (FLIM) of green fluorescent protein (GFP)[19] with sensitivity over length scales on the order of 3 μm.[20] In comparison, plasmonic NPs are sensitive to RI over length scales of tens of nanometers, potentially yielding

Address all correspondence to Adam Wax, Biomedical Engineering, Duke Univ., Box 90281, Durham, NC 27708; Tel: 919 660–5143; Fax: 919 684-4488; E-mail: a.wax@duke.edu

1083-3668/2008/13(1)/014022/7/$25.00 © 2008 SPIE

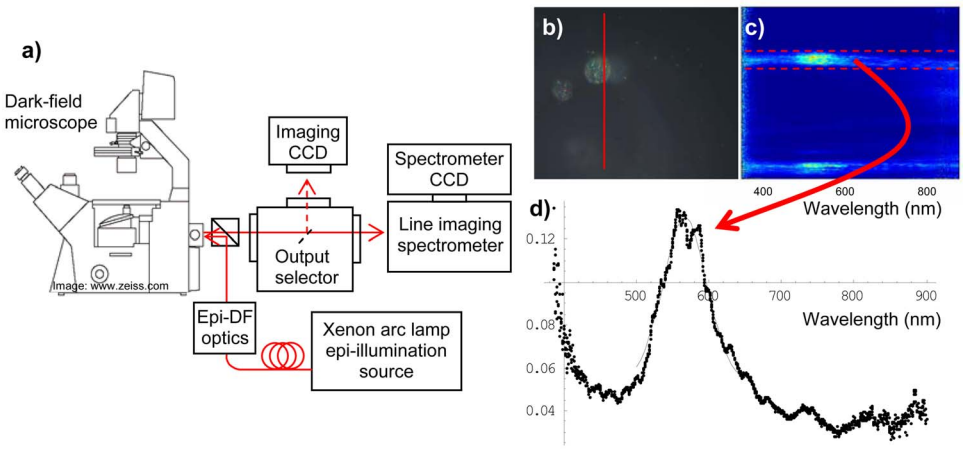

Fig. 1 (a) Measurement scheme for dark-field analysis of live cells in culture. (b) Color image of anti-EGFR conjugated NPs bound by EGFR-overexpressing A431 cell. (c) Corresponding false color spectral image acquired through red line in (b). (d) Average scattering spectrum from outlined region of spectral image. (Color online only.)

RI measurements with a spatial resolution 2 orders of magnitude better than the FLIM-based method. Further, since plasmonic NPs do not photobleach, they avoid the lifetime limitations of fluorescent tags, enabling intracellular RI monitoring over longer time scales.

We present here the results of a study in which 60-nm-diam gold nanospheres labeled with antiepidermal growth factor receptor (anti-EGFR) are used to molecularly image EGFR in live A431 cells. We measure and analyze the wavelength distribution of light scattered by bound NPs to determine local RI over nanometer length scales within the cells. To demonstrate the distinct difference in RI environment for receptor-mediated uptake, the results are compared to the scattering spectra of antibody-free NPs, taken up by cells through nonspecific mechanisms. The antibody-free NP data indicate the presence of interparticle effects that are not seen with the labeled NPs. We discuss this finding within the framework of refining future experimental schemes to enable high resolution intracellular RI mapping with NPs.

2 Materials and Methods

2.1 *Experimental Setup*

Scattering spectra are acquired using an optical dark-field microspectroscopy system[21] (Fig. 1), based on an inverted microscope (Axiovert 200, Carl Zeiss, Inc., Thornwood, New York) connected to a color camera (CoolSnap cf, Photometrics, Tuscon, Arizona) and a line-imaging spectrometer (SpectraPro 2150i, Acton Research, Trenton, New Jersey). The spectrometer is equipped with an imaging charge-coupled device (CCD) (Spec-10, Roper Scientific, Duluth, Georgia) to collect a stack of spectra through a selected line in the sample image. We have designed and implemented an epi-illumination dark-field light train,[22] enabling dark-field analysis of cells in culture. This illumination scheme provides enhanced contrast for NP scattering measurements of cells in culture media, as compared with transmitted dark-field illumination, where contrast is reduced by forward-scattered light from cellular organelles. The epi-illumination system also allows concurrent bright-field imaging for determining NP location relative to cell boundaries.

2.2 *Cell Culture*

A431 cells (Duke Cell Culture Facility) were maintained at 37 °C, in a 5% CO_2 atmosphere in Dulbecco's modified Eagle's medium with 4-mM L-glutamine adjusted to contain 1.5-g/L sodium bicarbonate and 4.5-g/L glucose, with 10% fetal bovine serum and 1% penicillin streptomycin. MDA-MB-453 (Duke Cell Culture Facility) cells were maintained at 37 °C in a 100% air atmosphere in Leibovitz's L-15 medium with 2-mM L-glutamine, with 10% fetal bovine serum and 1% penicillin streptomycin. For analysis on the microspectroscopy system, cells were suspended in 1 mL of media (or media and NPs) and plated to 2.0-mL chambered coverglasses (Lab-Tek). For studies with antibody-conjugated NPs, 80,000 cells per chamber were plated, while for studies with antibody-free NPs, 40,000 cells per chamber were plated. Plated cells were incubated 12 to 16 h, allowing cell adhesion to the substrate, but not confluence.

2.3 *Antibody-Nanoparticle Conjugation*

The antibody conjugation protocol for 60-nm Au spheres was adapted from protocols published for 12-nm[23] and 30-nm[5] Au spheres. For this protocol, 1 mL of 60-nm-diam Au colloid (Ted Pella, Incorporated) was diluted with 125-μL 20-mM HEPES buffer. Separately, 30-μL anti-EGFR mAb (E2156, Sigma) was diluted in 20-mM HEPES buffer to prepare a 3% (v/v) anti-EGFR solution. The pH values of the colloid and antibody preparations were then adjusted to 7.0+/−0.2 by addition of 100-nM K_2CO_3. The pH-adjusted colloid and antibody preparations were then mixed and allowed to conjugate at room temperature for 20 min on an oscillator operating at 190 cycles/min. To verify antibody attachment, 200 μL of the resulting conjugated colloid was removed and mixed with 10 μL of 10% NaCl. It is well known that addition of NaCl will cause nanoparticle aggregation,[24] resulting in a color

change to the solution, unless the NP surface has been well coated. After verifying that the NaCl did not produce a color change in the colloid, 200 μL of 1% polyethylene glycol (PEG) compound (Sigma P2263) was added to the remainder of the conjugated NP suspension and allowed to interact for 10 min. At the end of this interaction period, the solution was centrifuged at 6000 RPM until a pellet was formed ($\sim$10 min). The supernatant was then withdrawn, and the NP pellet was resuspended in 0.5 mL of phosphate buffered saline.

2.4 *Antibody-Free Nanoparticle Preparation*

To prepare similar NPs for the control experiment, the prior protocol was adapted with the exception of the EGFR antibody. 1 mL of 60-nm-diam Au colloid was diluted with 1.125-mL 20-mM HEPES buffer. 200 μL of 1% PEG compound was added to the resulting NP suspension and allowed to interact for 10 min. At the end of this interaction period, the solution was centrifuged at 6000 RPM until a pellet was formed ($\sim$10 min). The supernatant was then withdrawn, and the NP pellet was resuspended in 0.5 mL of phosphate buffered saline, resulting in a concentration of $\sim 2 \times 10^{10}$/ml.

2.5 *Cell Treatment with Nanoparticles*

Cells designated for testing with antibody-conjugated NPs (A431 and MDA-MB-453) were incubated overnight in pure media, as described before, to allow cell adhesion. The media was then exchanged with 0.5-mL NP suspension (1.3 optical density in a 1-cm path-length cuvette) mixed with 0.5-mL fresh media and incubated for 20 min. At the end of this incubation period, the media was removed, and fresh media was used to rinse the cells twice. Fresh media was added once more, and analysis on the microspectroscopy system was conducted immediately at room temperature. Cells designated for testing with antibody-free NPs (A431 only) were incubated overnight in 0.5-mL pure media plus 0.5-mL antibody-free NP suspension (0.6 optical density). We note that the longer incubation period was needed to observe any uptake of NPs by the cells. After incubation, the media on the cells was then withdrawn, and fresh media was used to rinse the cells twice. Fresh media was added, and analysis on the microspectroscopy system was conducted immediately at room temperature.

2.6 *Nanoparticle Extinction Measurements*

Characterization of NP suspensions was performed using a fiber-coupled linear CCD spectrometer (Ocean Optics USB2000) and halogen light source (Ocean Optics LS-1) to execute transmission measurements. Extinction spectra of pure NP colloid and conjugated NP suspensions were acquired in a 1-cm path-length cuvette. Measurement of NP scattering spectra in cell cultures was performed with the microspectroscopy system described earlier. Spectra were analyzed by fitting a Gaussian function to the spectral peak and extracting the center wavelength of the fitting function.

2.7 *Nanoparticle Optical Property Modeling*

NP optical properties were modeled with an extension to Mie theory for coated spheres implemented in Matlab with publicly available code.[25] The measurements of Blanchard et al.[26] were used for the wavelength-dependent complex dielectric function of gold. Wavelength invariance was assumed for the dielectric properties of all other materials. The standard deviation in the size of the NPs was assumed to be 3.1 nm, based on manufacturer-provided specifications. NP mean size was determined by fitting the measured extinction spectrum using the theory for uncoated NPs and found to agree with manufacturer specifications. The RI of the antibody layer was determined by fitting the measured extinction spectrum for coated NPs using the model for scattering by a coated sphere, with the coating thickness measured by TEM. The RI layer thickness in subsequent preparations was determined by fitting the preparation's measured extinction spectrum to the model, assuming the antibody layer RI, as determined earlier. The cellular RI environment was determined by fitting the mean scattering peak for NPs in cells to the model for scattering by a coated sphere, assuming the input parameters determined before and using the ambient RI as the free parameter.

The total uncertainty in cellular RI environment was calculated by orthogonal summation of the component parameter uncertainties, according to the following equation:

$$\Delta n_{\mathrm{cell}}^2 = \left(\frac{d}{dr} n_{\mathrm{cell}} \cdot \Delta r\right)^2 + \left(\frac{d}{dt_{\mathrm{coat}}} n_{\mathrm{cell}} \cdot \Delta t_{\mathrm{coat}}\right)^2 + \left(\frac{d}{dn_{\mathrm{coat}}} n_{\mathrm{cell}} \cdot \Delta n_{\mathrm{coat}}\right)^2 + \left(\frac{d}{d\lambda_{\mathrm{sca}}} n_{\mathrm{cell}} \cdot \Delta \lambda_{\mathrm{sca}}\right)^2,$$

where Δx is the uncertainty in x and the differential dy/dz is the measured dependence of a change in y due to a change in z. The uncertainty in each derived parameter in the equation was also calculated by orthogonal summation of its component parameter uncertainties, with measured differentials. In this way, the uncertainty of each derived parameter was traced to the uncertainty in measured parameters. The impact of these uncertainty calculations is considered in Sec. 4.

2.8 *Transmission Electron Microscopy (TEM)*

Cells were prepared for TEM analysis by *in-situ* fixation on the coverslip in 4% glutaraldehyde, post-fixation in 1% osmium tetroxide, and *en bloc* staining in 1% uranyl acetate. Serial dehydration in ethanol was performed at concentrations of 35, 70, 95, 100, and 100%. Impregnation was performed with a 50/50 mix of epon resin and 100% ethanol, followed by two exchanges of 100% epon resin. Resin was polymerized on the coverslip at 70 °C overnight. The resin film with cells was removed from the coverslip, and selected areas were mounted on a resin stub for sectioning. Thin sections were cut on a Reichert UltraCut S ultramicrotome and mounted on 200 mesh copper/rhodium grids. Sections were stained with 2% uranyl acetate and 1% lead citrate. Nanoparticles were prepared for TEM analysis by exposure of colloid to Formvar grids, followed by staining with 2% uranyl acetate and 1% lead citrate. Samples were viewed on a Philips CM 12 TEM, and images were captured on an Advanced Microscopy Techniques (Danvers, Massachusetts) digital camera system.

3 Results

To establish molecularly specific uptake of NPs, we compare the results from the conjugated NP experiments with three

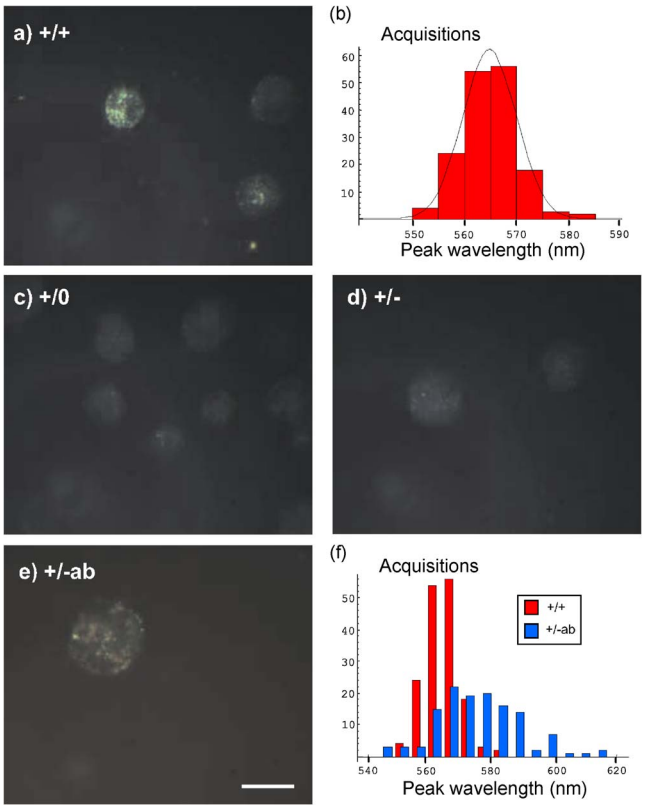

Fig. 2 Results from dark-field imaging and spectral analysis of molecular specific NP tagging. (a) Dark-field image of (+/+) experiment, showing strong green scattering from anti-EGFR NPs bound to A431 cells. Note that the reduced scattering intensity from cells in the peripheral region is caused by reduced dark-field illumination there, rather than the lack of NP binding. (b) Distribution of peak wavelengths for anti-EGFR conjugated NPs bound to A431 cells. The vertical axis gives number of spectra (total N=161). (c) and (d) Dark-field images for control experiments, showing no evident NP binding: (c) A431 cells with no NP exposure (+/0); and (d) A431 cells incubated with NPs conjugated with negative control antibody (+/-), which appear identical to EGFR nonexpressing MDA-MB-453 cells incubated with anti-EGFR conjugated NPs (-/+) (not shown). (e) Dark-field image of NPs prepared without antibody (+/-ab) in A431 cells. (f) Distribution of peak scattering wavelengths showing red-shifted and broadened distribution for A431 incubation with antibody-free NPs incubated (+/-ab, n=128) versus anti-EGFR conjugated NPs (+/+, n =161). Scale bar represents 20 μm for all images. (Color online only.)

control sets. As shown in Fig. 2(a), dark-field imaging of A431 cells, which overexpress EGFR upon incubation with anti-EGFR NPs (denoted as the +/+ experiment), shows significant NP retention following a 20-min incubation period, consistent with the expected antibody interaction. Figures 2(c) and 2(d) show typical results from the negative control experiments. Figure 2(c) shows dark-field images of A431 cells with no exposure to NPs (+/0). Figure 2(d) shows dark-field images of the A431 cells after incubation with NPs conjugated to an isotype-matched negative control antibody (+/−). Finally, similar experiments with MDA-MB-453 cells, known to not express EGFR,[27] exposed to the anti-EGFR conjugated NPs (−/+) show no noticeable NP retention (data not shown), and are nearly indistinguishable from the untreated control cells [Fig. 2(c)]. The peak wavelength of the NP scattering spectra after NP binding to cell surface receptors were found to be fairly consistent across the analyzed cells. To determine the peak of the scattering spectrum, the spectral image is averaged (Fig. 1) across a region of interest, corresponding to a line through a cell. The scattering data are normalized by the source spectrum obtained by using the spectra from adjacent slit positions at which there are no NPs or cells present, as described previously.[22] The resonance peak is determined by fitting the averaged spectrum using a Gaussian function. The peak wavelengths from the 161 image acquisitions in the +/+ experiment are shown in Fig. 2(b) and are seen to be normally distributed, with a mean peak wavelength of 564.8 nm and standard deviation of 5.0 nm.

Intracellular RI sensing is achieved by analyzing the distribution of peak wavelengths in the NP scattering spectra to relate them to the RI nanoenvironment. To determine the RI with any degree of certainty, it is essential that the NP samples are well characterized. We have used theoretical models of NP absorption and scattering (Mie theory and its extension for coated spheres[28]) to precisely determine the NP size distribution as well as thickness and RI of the antibody layer. The characterization begins by determining the average diameter of the untreated NPs by fitting the measured extinction spectrum of the NP colloid to the Mie theory model. In these experiments, the NP preparation was found to have a mean diameter of 65.6 nm+/−0.04 nm. Here, the uncertainty in the mean diameter is obtained from the fitting to the size distribution. The standard deviation in NP size was assumed to be that given by the manufacturer of 3.1 nm (see Sec. 2.7).

To model the scattering by the antibody-coated NPs, the RI of the antibody layer is needed. This parameter is determined to be 1.44+/−0.04 by fitting the extinction spectrum of a sample of coated NPs using the coated sphere model, with the antibody layer thickness measured to be 3.1+/−0.7 nm directly via transmission electron microscopy [TEM, see Fig. 3(b)]. The thickness of the antibody layer adsorbed on subsequent NP preparations can then be easily determined by analyzing their measured extinction spectrum with the coated sphere model. For the preparation used in the cell experiments, the antibody layer thickness was determined to be 4.1+/−1.8 nm. We note that this thickness is less than the length of an individual antibody (~12 nm), with the difference most likely due to the average of the random orientation of the antibody relative to the NP. Incomplete coverage of the NP surface could also result in an average thickness that is less than the length of the antibody.

Due to the possible influence of the dry environment during the TEM measurements, as compared to the aqueous environment of the NPs in suspension, we have sought to confirm the NP coating thickness using an alternative method, dynamic light scattering (ZetaPlus, Brookhaven Instruments Corporation, Holtsville, New York). In these experiments, a new batch of NPs was tested both before and after executing the conjugation protocol described before. The mean diameter determined for the bare NPs was 70.7+/−0.4 nm, while the mean diameter of the coated NPs was found to be 77.7+/−0.5 nm. This indicates that the achieved coating thickness for this batch of conjugated NPs was 3.6+/−0.4 nm. Thus, the antibody thickness found using dynamic light scattering is consistent with the values reported earlier for the other NP

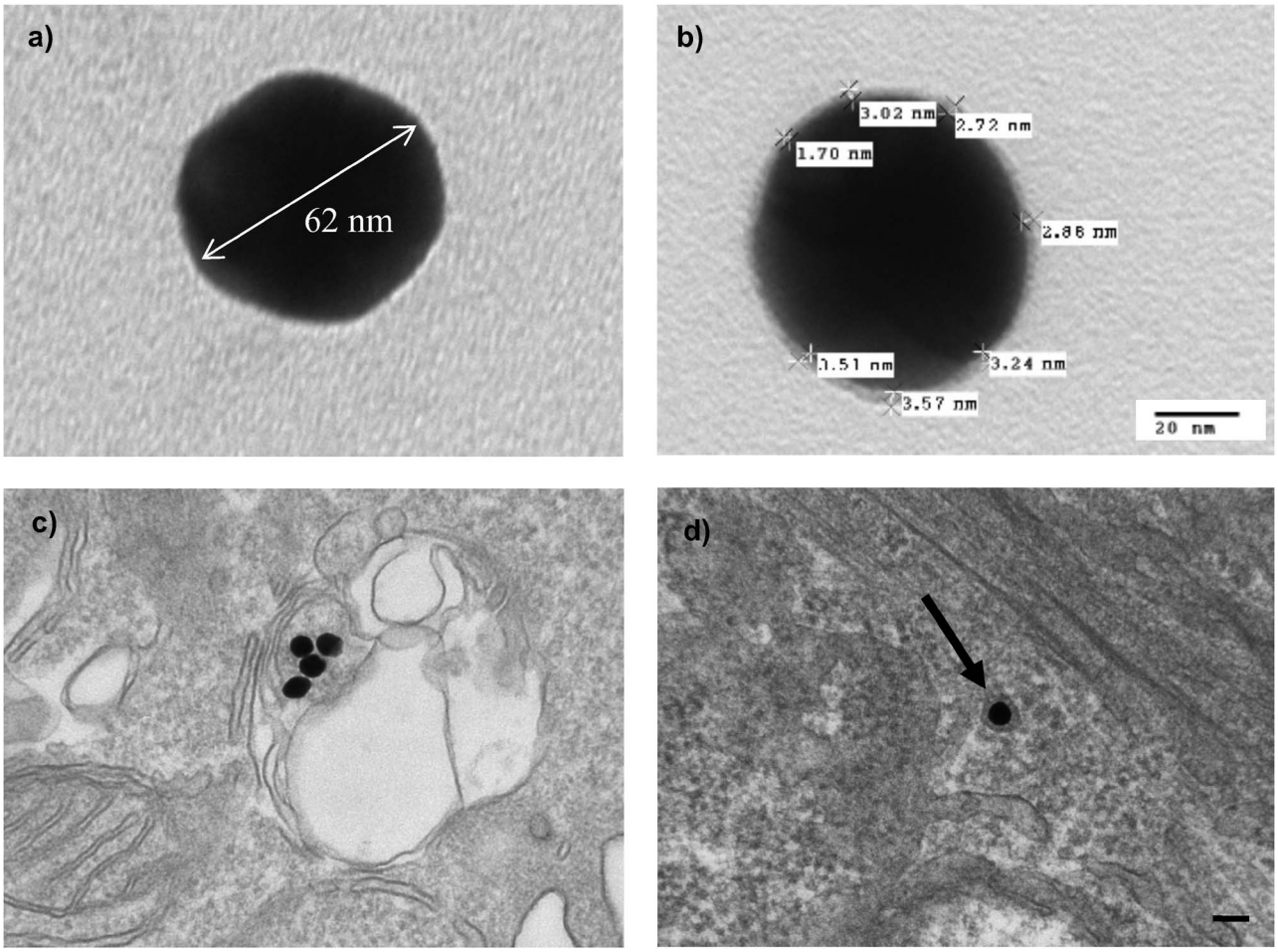

Fig. 3 Representative TEM images of NPs. (a) and (b) Scale bar represents 20 nm. (a) TEM image of bare NP, showing no antibody layer. (b) TEM image of anti-EGFR conjugated NP, showing antibody layer thickness measurements. Thickness measurement allows determination of antibody layer RI, which was needed for interpreting scattering spectra from NPs incubated with cells. (c) and (d) Scale bar represents 100 nm. (c) TEM image of antibody-free NPs incubated with A431 cells, showing NP aggregation in endocytic vesicles. The NP aggregation likely causes the red-shifted spectra measured for antibody-free NPs. (d) TEM image of anti-EGFR NPs incubated with A431 cells, showing NP isolation in vesicles (indicated by arrows) formed during receptor internalization. The narrow distribution of measured peak wavelengths is consistent with the uniform RI environment created by NP isolation and encapsulation in vesicles. (Color online only.)

preparations, and this additional data alleviates potential concerns arising from comparing wet and dry measurements. For this NP preparation, the extinction measurements for the bare NPs showed a peak scattering wavelength of 537.0 nm, which gives a mean diameter of 72.0+/−0.4 nm via fitting with Mie theory. The mean diameter of the bare NPs and the thickness of the coating are then used to extract the RI of the coating using Mie theory for coated spheres. From this additional data, we determine the RI to be 1.42+/−0.04, a finding consistent with the value reported before that was used for RI determination.

Finally, after the thorough characterization, the NP preparation is delivered to cells. The resulting scattering spectra are then measured and used to determine the intracellular RI. The uncertainty in the RI determination is assessed by considering the uncertainties in each parameter used. From the scattering data, the intracellular RI for the nanoenvironment of anti-EGFR labeled NPs bound to EGFR on A431 cells is found to be 1.53+/−0.02.

To investigate the influence of uptake mechanism on NP intracellular environment, we also measured scattering spectra of antibody-free NPs nonspecifically taken up by A431 cells [Fig. 2(e), +/−ab] during an overnight incubation period. To observe any uptake of the antibody-free NPs, a significantly longer incubation period was needed compared to that used for antibody-conjugated NPs. Comparison of the peak scattering wavelength distributions for the antibody-free and antibody-conjugated NPs [Fig. 2(f)] reveals a difference with high statistical significance ($p < 0.0001$), indicating different nanoenvironments. The origin of the difference in peak wavelength distributions is discussed next.

4 Discussion

The nanoenvironment experienced by anti-EGFR NPs bound to EGFR in A431 cells has been found to have a RI of 1.53 +/−0.02. Previous studies have investigated RI of cellular components with significantly lower spatial resolution. These

studies cite RI values of 1.46 to 1.6 for cell membrane[10–12,20] and 1.35 to 1.39 for cytoplasm.[11,13,14] The RI of proteins has been cited as 1.36 to 1.55.[29] The RI values that we have determined for the NPs' cellular environment, as well as that found for the NP antibody layer, are consistent with the values cited for cell membrane and proteins. The intracellular RI measurement presented here is the first determination of RI within suboptical resolution volumes in living cells, to our knowledge. By considering the extent of NP sensitivity to be twice the 1/e sensing range (0.7 times the radius[9]), the RI sensing volume is estimated to be 1.5 attoliters, or about 3E-6 times the volume of a 10-μm-diam spherical cell. Sensing volumes on this order may provide exceptionally detailed mappings of intracellular environments and monitoring of cellular dynamics.

The total uncertainty in the RI measurement (0.02 RIU) can provide insight into improving the precision of NP-based intracellular sensing by identifying the dominant sources of uncertainty in the RI determination. The individual extinction measurements used to characterize NP suspensions each have an uncertainty of 0.027 nm when determining peak wavelength, calculated as described previously.[30] The average peak wavelength for light scattered by NPs in cells is determined with an uncertainty of 0.4 nm, given by the standard error of the mean for the distribution of measured scattering peaks. The determination of antibody RI and layer thickness has uncertainties of 0.04 RIU and 1.8 nm, respectively, which are calculated from the uncertainties in their requisite modeling parameters. As an estimate of possible improvement, using 60-nm nanospheres with size uncertainty of 1%, coated with antibody layers with thickness variations of 0.5 nm, the total uncertainty for a single NP measurement could be reduced to less than 0.01 RIU.

Analysis of the parameters that comprise the total uncertainty of the intracellular RI determination indicates that the dominant factor is the variation in antibody layer thickness, which serves to broaden the distribution of peak scattering wavelengths. The distribution of peak scattering wavelengths is in fact broadened by any NP heterogeneity, including variations in size, shape, and antibody layer thickness. Therefore, minimizing variations in the NP preparation will enable more precise measurements of intracellular RI environment. Further, by reducing variations in NP preparation, it may be possible to identify changes in the spectra of individual NP spectra due to the RI nanoenvironment, in contrast to the ensemble averaged method presented here. Using individual NPs to assess intracellular RI will enable precise measurements in suboptical resolution regions of interest. Although RI is not currently a common marker used for cellular studies, it is possible that introduction of a precise intracellular RI sensor will open new avenues for application of RI to cell morphology and cell dynamics studies.

A significant finding presented here is the difference between the RI nanoenivronments experienced by the NPs due to the uptake mechanism. Comparison of the scattering distributions for the antibody-free and antibody-conjugated NPs indicates substantially different nanoenvironments. However, analysis to determine the RI nanoenvironment of the antibody-free NPs is complicated by the fact that many of the peak wavelengths for these NPs yield RI values that we do not consider realistic for cellular environments, suggesting the possibility of interparticle plasmon coupling. A recent study by Aaron et al.[31] has shown that plasmon coupling can become significant when high concentrations of NPs are bound to the cell membrane for NP-based molecular imaging. We avoid the effect of plasmon coupling in this study by using a 100× lower concentration of NPs than that used by Aaron et al. We are able to execute molecular imaging using a significantly lower concentration, because our epi-illumination train for dark-field microspectroscopy is effective at suppressing endogenous cell scatter.[22] This lower background level enables a higher sensitivity to NP scattering compared to transmission dark-field microscopy schemes such as those used in Ref. 31.

To investigate the likelihood of interparticle plasmon coupling between antibody-free NPs, a sample of treated cells was imaged with TEM. These images show that antibody-free NPs are localized to endocytic vesicles containing aggregations of several NPs [Fig. 3(c)]. This result stands in contrast with the TEM images of cells incubated with anti-EGFR conjugated NPs, which show NPs individually localized to vesicles, likely formed during receptor internalization [Fig. 3(d)]. Due to the low concentration of NPs used in these experiments and the thin sectioning required for TEM imaging, very few NPs were observed in these images. However, for all TEM images of cells incubated with anti-EGFR conjugated NPs, where NPs were observed (N=4 images), they appeared as individual NPs, isolated in endocytic vesicles similar to that shown in Fig. 3(d). The resultant consistency in RI nanoenvironment explains the narrow distribution of peak wavelengths observed for the antibody-conjugated NPs. In contrast, for the antibody-free NPs, a broad range of scattering peaks is observed. Thus, because of NP aggregation, an accurate RI determination cannot be made with the antibody-free NPs.

The aggregation of antibody-free NPs in cells observed in the TEM images is consistent with the assertion that interparticle plasmon coupling causes the relatively high peak scattering wavelengths observed. These interparticle effects cannot be modeled with standard Mie theory, but a multipole method has been developed to model these effects by considering interparticle interactions as a superposition of vector spherical harmonics about each sphere.[32] A multipole-based simulation of two nanospheres at separation distances on the order of a particle radius in an aqueous (n=1.33) environment yields peak scattering wavelengths that are consistent with the measured peak wavelengths.[33] These results indicate that our measurements of antibody-free NPs are influenced both by RI environment and interparticle effects, unlike the antibody-conjugated NPs.

In conclusion, we demonstrate a dark-field microspectroscopy technique for molecular imaging of live cells using immuno-labeled plasmonic NPs. By also obtaining the spectrum of scattered light, additional functional information is obtained beyond simple contrast enhancement. Here, the scattering spectra of labeled NPs bound by cell surface receptors are used for the first determination of intracellular RI in attoliter volumes within live cells. Comparison of spectral measurements from antibody-conjugated NP and antibody-free NPs has revealed that interparticle plasmon coupling can affect property determination. Further development of the tech-

nique will require optical discrimination of interparticle effects and improved NP synthesis, and conjugation processes to yield more homogenous preparations. More tightly controlled NP preparations will enable a broad range of precision single NP intracellular RI measurements. Advancing the approach in this manner will facilitate improved modeling of cell and tissue optical properties, monitoring of cellular dynamics, and improved long-term tracking of targeted NPs within cells.

Acknowledgments

We would like to thank Anne Lazarides and David Sebba for performing the multipole simulations; Ashutosh Chilkoti and Molly Miller for fruitful discussions; Mark Gu for assistance with cell culture; Phillip Christopher for assistance with TEM; and the Beverley and Clarence Chandran Research Award for financial support.

References

1. S. Schultz, D. Smith, J. Mock, and D. Schultz, "Single-target molecule detection with nonbleaching multicolor optical immunolabels," *Proc. Natl. Acad. Sci. U.S.A.* **97**(3), 996–1001 (2000).
2. E. E. Connor, J. Mwamuka, A. Gole, C. J. Murphy, and M. D. Wyatt, "Gold nanoparticles are taken up by human cells but do not cause acute cytotoxicity," *Small* **1**(3), 325–327 (2005).
3. B. D. Chithrani, A. A. Ghazani, and W. C. W. Chan, "Determining the size and shape dependence of gold nanoparticle uptake into mammalian cells," *Nano Lett.* **6**(4), 662–668 (2006).
4. C. Loo, A. Lowery, N. Halas, J. West, and R. Drezek, "Immunotargeted nanoshells for integrated cancer imaging and therapy," *Nano Lett.* **5**(4), 709–711 (2005).
5. I. El-Sayed, X. Huang, and M. El-Sayed, "Surface plasmon resonance scattering and absorption of anti-EGFR antibody conjugated gold nanoparticles in cancer diagnostics: Applications in oral cancer," *Nano Lett.* **5**(5), 829–834 (2005).
6. C. Sonnichsen, B. Reinhard, J. Liphard, and A. Alivisatos, "A molecular ruler based on plasmon coupling of single gold and silver nanoparticles," *Nat. Biotechnol.* **23**(6), 741–745 (2005).
7. A. Haes, W. Hall, L. Chang, W. Klein, and R. Van Duyne, "A localized surface plasmon resonance biosensor: First steps toward an assay for Alzheimer's disease," *Nano Lett.* **4**(6), 1029–1034 (2004).
8. N. Nath and A. Chilkoti, "Label free colorimetric biosensing using nanoparticles," *J. Fluoresc.* **14**(4), 377–389 (2004).
9. M. Miller and A. Lazarides, "Controlling the sensing volume of metal nanosphere molecular sensors," *Mater. Res. Soc. Symp*, Warrendale, PA (2004).
10. J. Beuthan, O. Minet, J. Helfmann, M. Herrig, and G. Muller, "The spatial variation of the refractive index in biological cells," *Phys. Med. Biol.* **41**(3), 369–382 (1996).
11. S. Johnsen and E. A. Widder, "The physical basis of transparency in biological tissue: Ultrastructure and the minimization of light scattering," *J. Theor. Biol.* **199**(2), 181–198 (1999).
12. R. A. Meyer, "Light-scattering from biological cells—dependence of backscatter radiation on membrane thickness and refractive-index," *Appl. Opt.* **18**(5), 585–588 (1979).
13. J. A. C. Valkenburg and C. L. Woldringh, "Phase-separation between nucleoid and cytoplasm in Escherichia-Coli as defined by immersive refractometry," *J. Bacteriol.* **160**(3), 1151–1157 (1984).
14. K. Sokolov, R. Drezek, K. Gossage, and R. Richards-Kortum, "Reflectance spectroscopy with polarized light: is it sensitive to cellular and nuclear morphology," *Opt. Express* **5**(13), 302–317 (1999).
15. R. Barer, "Refractometry and interferometry of living cells," *J. Opt. Soc. Am.* **47**(6), 545–556 (1957).
16. *Handbook of Chemistry and Physics*, 85 ed., D. Lide, ed. CRC Press, Boca Raton, FL (2004).
17. C. L. Curl, C. J. Bellair, T. Harris, B. E. Allman, P. J. Harris, A. G. Stewart, A. Roberts, K. A. Nugent, and L. M. D. Delbridge, "Refractive index measurement in viable cells using quantitative phase-amplitude microscopy and confocal microscopy," *Cytometry* **65**(1), 88–92 (2005).
18. N. Lue, G. Popescu, T. Ikeda, R. R. Dasari, K. Badizadegan, and M. S. Feld, "Live cell refractometry using microfluidic devices," *Opt. Lett.* **31**(18), 2759–2761 (2006).
19. M. Miller and A. Lazarides, "Nanoengineered assemblies and advanced micro/nanosystems," D. P. Taylor et al., eds., *Mater. Res. Soc. Symp. Proc.* **820**, 407–413 (2004).
20. C. Jones and K. Suhling, "Refractive index sensing using Fluorescence Lifetime Imaging (FLIM)," in *2nd Intl. Conf. Opt. Laser Diagnostics*, Institute of Physics. (2005).
21. A. Curry, G. Nusz, A. Chilkoti, and A. Wax, "Substrate effect on refractive index dependence of plasmon resonance for individual silver nanoparticles observed using darkfield micro-spectroscopy," *Opt. Express* **13**(7), 2668–2677 (2005).
22. A. Curry, W. L. Hwang, and A. Wax, "Epi-illumination through the microscope objective applied to darkfield imaging and microspectroscopy of nanoparticle interaction with cells in culture," *Opt. Express* **14**(14), 6535–6542 (2006).
23. K. Sokolov, M. Follen, J. Aaron, I. Pavlova, A. Malpica, R. Lotan, and R. Richards-Kortum, "Real-time vital optical imaging of precancer using anti-epidermal growth factor receptor antibodies conjugated to gold nanoparticles," *Cancer Res.* **63**(9), 1999–2004 (2003).
24. K. Sato, K. Hosokawa, and M. Maeda, "Rapid aggregation of gold nanoparticles induced by non-cross-linking DNA hybridization," *J. Am. Chem. Soc.* **125**(27), 8102–8103 (2003).
25. C. Matzler, *MATLAB Functions for Mie Scattering and Absorption*, Univ. of Bern, Institute of Applied Physics, Bern, Switzerland (2002).
26. N. P. Blanchard, C. Smith, D. S. Martin, D. J. Hayton, T. E. Jenkins, and P. Weightman, "High-resolution measurements of the bulk dielectric constants of single crystal gold with application to reflection anisotropy spectroscopy," *Phys. Status Solidi C* **0**(8), 2931–2937 (2003).
27. Y. Yarden, and R. A. Weinberg, "Experimental approaches to hypothetical hormones: Detection of a candidate ligand of the neu protooncogene," *Proc. Natl. Acad. Sci. U.S.A.* **86**(9), 3179–3183 (1989).
28. C. F. Bohren and D. R. Huffman, *Absorption and Scattering of Light by Small Particles*, Wiley, New York (1983).
29. J. Voros, "The density and refractive index of adsorbing protein layers," *Biophys. J.* **87**(1), 553–561 (2004).
30. A. Curry, G. Nusz, A. Chilkoti, and A. Wax, "Analysis of total uncertainty in spectral peak measurements for plasmonic nanoparticle-based biosensors," *Appl. Opt.* **46**, 1931–1939 (2007).
31. J. Aaron, N. Nitin, K. Travis, S. Kumar, T. Collier, S. Y. Park, M. Jose-Yacaman, L. Coghlan, M. Follen, R. Richards-Kortum, and K. Sokolov, "Plasmon resonance coupling of metal nanoparticles for molecular imaging of carcinogenesis in vivo," *J. Biomed. Opt.* **12**(3), 034007 (2007).
32. D. W. Mackowski, "Calculation of total cross sections of multiple-sphere clusters," *J. Opt. Soc. Am. A* **11**(11), 2851–2861 (1994).
33. A. Lazarides and D. Sebba, private communication, Duke University (2007).